

## Static Light Scattering Studies on Xanthan in Aqueous Solutions

Gisela Berth,<sup>\*,†</sup> Herbert Dautzenberg,<sup>‡</sup> Bjørn E. Christensen,<sup>†</sup> Stephen E. Harding,<sup>§</sup> Gudrun Rother,<sup>‡</sup> and Olav Smidsrød<sup>†</sup>

Norwegian Biopolymer Laboratory (NOBIPOL), Department of Biotechnology, University of Trondheim, NTH, N-7034 Trondheim, Norway, Max Planck Institute for Colloid and Interface Science, D-14513 Teltow, Germany, and Department of Applied Biochemistry and Food Science, University of Nottingham, Sutton Bonington LE12 5RD, U.K.

Received October 16, 1995; Revised Manuscript Received February 20, 1996<sup>®</sup>

**ABSTRACT:** A commercial sample of xanthan was (i) sonicated and fractionated by GPC on Sepharose Cl-2B with 0.1 M NaCl as eluant/solvent. The angular dependence of scattered light was measured (off-line) and interpreted in terms of the wormlike chain model using the "master curve procedure". The persistence length was estimated as  $L_p \approx 150$  nm. The mass per unit length  $M_L \approx 2000$  g/mol·nm indicates double-stranded chains. (ii) The parent sample was studied at various ionic strengths  $I$  ( $0.01 \text{ mol/L} \leq I \leq 0.3 \text{ mol/L}$ ). The conditions for optimum solubility and clarification (ultracentrifugation/membrane filtration) were checked. At higher ionic strength, the sample was only partly soluble and the solution contained supermolecular structures even after clarification. Good solubility was observed in 10 mM NaCl. The Zimm procedure was used to obtain the average molar mass  $M_w$ , the second virial coefficient, and the radius of gyration  $R_g$ . The interpretation of the scattering function led to  $M_w = 2.88 \times 10^6$  g/mol,  $R_g = 241$  nm,  $L_p = 149$  nm, a polydispersity  $\sigma_M = 0.5$ , and double-stranded chains. At room temperature, solutions revealed a tendency for aggregation, which could be prevented by storage at elevated temperature.

### Introduction

Xanthan is a microbial polysaccharide. According to its chemical structure,<sup>1</sup> xanthan can be classified as stereoregular copolymeric polyelectrolyte. It shares the backbone with cellulose. The conformation of xanthan in aqueous solution has been the subject of controversy for a long period of time but it seems to have become a certainty that the native form consists of double-stranded stiff chains.<sup>2–9</sup> The interpretation of experimental data from sedimentation analysis, static light scattering, and viscosity measurements in terms of the wormlike chain model has led to a persistence length  $L_p = (120 \pm 20) \text{ nm}^{3-5}$  or higher.<sup>10</sup> A recently presented interpretation of the angular dependence of scattered light<sup>11</sup> suggested more flexible chains with  $L_p$  in the range of 55–70 nm.

Many investigations with the aim of studying the conformation and its stability/variability upon variable experimental conditions (salinity, temperature) have been performed on relatively low molar mass sample series ( $M_w \leq 10^6$  g/mol) which had been prepared by either sonication or fractionation (GPC) from degraded (by sonication) parent samples.<sup>2–7,11</sup> Such samples have allowed study of the conformation without interference from problems arising from a limited solubility. High molecular weight samples have frequently revealed only partial solubility at ionic strengths of 10 mM and above where the solubility decreases with increasing salinity.<sup>11–13</sup> A variety of Mark–Houwink–Kuhn–Sakurada equations have been established (reviewed in ref 14). At least in part, a different treatment of samples prior to the determination of molar masses can

be assumed to play a role beyond the varying degree of substitution with pyruvate and acetate and the salinity of the solvent (see, e.g., refs 15 and 16). Light scattering measurements are extremely sensitive to even traces of incompletely dissolved or partly aggregated material or, more generally expressed, to every kind of supermolecular or large extraneous contamination. Poorly reproducible and unexpectedly low second virial coefficients  $B$  such as in ref 13 as well as the lack of a relationship between the molar mass  $M_w$  and the radius of gyration  $R_g$ <sup>15</sup> suggest that the preparation of solutions which contain solely molecularly dispersed species seems to be a problem in the case of high molecular weight samples. A combination of centrifugation and subsequent membrane filtration has become common practice for clarification<sup>2,12,15</sup> but both the conditions of centrifugation (duration, speed) and pore size of membrane filters have been found to affect results.<sup>13,15</sup> A loss of 25% of the original matter was observed after centrifugation at  $I = 0.5 \text{ mol/L}$ .<sup>13</sup> However, systematic studies on the effects of clarification—step by step—are not available. Thus, being faced with the estimation of the molar mass by static light scattering (SLS), one cannot refer to any standard procedure but has to discover the optimum conditions with respect to salinity and clarification by experiment.

The present paper reports results of SLS studies on a commercial xanthan sample at different ionic strengths  $I$  adjusted by added NaCl ( $0.01 \text{ mol/L} \leq I \leq 0.30 \text{ mol/L}$ ). The Zimm procedure<sup>17</sup> is used for the determination of  $M_w$ ,  $R_g$ ,  $B$ , and the scattering function  $P(\theta)$  at zero concentration. The angular dependence of scattered light will be discussed in terms of the wormlike chain model<sup>18,19</sup> by fitting with model curves. The polydispersity  $\sigma$  and the chain stiffness  $L_w/L_p$  (with  $L_w$  the weight-average contour length) are known to interfere (see, e.g., ref 20) so that an unambiguous assignment of effects is not possible<sup>21,22</sup> unless one or both can be determined separately. In recent studies on xylinan (acetan), we noticed that there was only little play in

\* To whom correspondence should be sent. Present address: Dr. G. Berth c/o Dr. H. Dautzenberg, MPI, Kantstrasse 55, D-14558 Teltow, Germany.

† Norwegian Biopolymer Laboratory.

‡ Max Planck Institute for Colloid and Interface Science.

§ University of Nottingham.

® Abstract published in *Advance ACS Abstracts*, April 1, 1996.

choosing appropriate pairs of  $L_w/L_p$  and  $\sigma_M$  for a fixed value of  $L_p$ . Moreover, also  $L_p$  could be varied in only narrow limits if a set of curves for homologous fractions with graduated molar masses was to be interpreted. Therefore, we will make use of the same procedure (see next paragraph) and analyze the same xanthan sample after sonication followed by fractionation (GPC on Sepharose Cl-2B) in order to obtain a reasonable value for  $L_p$ . For the parent sample, the polydispersity  $\sigma_M$  can then be estimated from the experimental scattering curve. This procedure can also be hoped to indicate minor amounts of particulate impurities which possibly may have remained or were re-formed after clarification and which would falsify especially the low-angle region of the commonly strongly curved scattering curves for xanthans.

For the interpretation of scattering curves, we will make use of the "master curve" procedure.<sup>23,24</sup> It has been developed for a sophisticated analysis of scattering curves of sufficiently large species ( $R_g \geq 100$  nm), the scattering curves of which contain information on the structure type and the polydispersity of the system. For a highly diluted polydisperse system of particles, the Rayleigh ratio of the scattering intensity is given by the simple expression

$$R_\theta(q) = M_w K c P_z(q) \quad (1)$$

with  $M_w$  the weight-average molar mass of the scattering particles,  $K$  a contrast factor containing the optical parameters of the system,  $c$  the mass concentration in g/mL, and  $P_z(q)$  the  $z$ -average of the intramolecular scattering function where the scattering vector  $q = (4\pi/\lambda) \sin(\theta/2)$  with  $\lambda$  the wavelength in the medium and  $\theta$  the scattering angle between incident and scattered beam.

Describing the polydispersity of the system by a continuous normalized mass distribution function  $p_w(M)$ , we obtain

$$M_w = \int_0^\infty M p_w(M) dM \quad (2)$$

and

$$P_z(q) = \frac{1}{M_w} \int_0^\infty P(q, M) M p_w(M) dM \quad (3)$$

where  $P(q, M)$  is the intraparticle scattering function for a particle of the molar mass  $M$ . Knowing  $P(q, M)$  and assuming a distribution function  $p_w(M)$ , we can calculate the scattering functions for polydisperse systems. The intraparticle scattering functions have been given for various basic structure types. The choice of a special distribution function for monomodal systems has been shown to be of minor importance for the scattering analysis.<sup>24</sup> We have used a special logarithmic distribution:

$$p_w(M) = \frac{M^{-3/2} \exp[-(\ln M - \ln M_w)/2\sigma_M^2]}{(2\pi)^{1/2} \sigma_M M_w^{-1/2} \exp[\sigma_M^2/8]} \quad (4)$$

which manages that  $M_w$  becomes independent of  $\sigma_M$ .

For a given structure type,  $p_w(M)$  and  $\sigma_M$  may easily be correlated with the characteristic size parameter of the particles (e.g., radius  $a$  for spheres or radius of gyration for coils) via the relation between mass and size. For small polydispersities,  $\sigma_M$  is equal to the

relative standard deviation and is given in general by  $M_w/M_n = \exp(\sigma_M^2)$ .

The theoretical basis of the master curve procedure is that (i) the scattering intensity  $R_\theta$  at  $\theta = 0$  ( $\theta$  is the angle of observation) is proportional to  $M_w$  and (ii) in the framework of the Rayleigh–Debye approximation, the intraparticle scattering function  $P_z(q)$  depends on the product of  $q$  ( $q = (4\pi/\lambda) \sin(\theta/2)$ ) with a characteristic size parameter  $a$ , the definition of which depends on the structure model used. Therefore, in a double-logarithmic plot of  $R_\theta/Kc$  versus  $qa$ , the change of  $M_w$  corresponds to a shift along the ordinate, with  $K$  the optical constant. The change of the size parameter corresponds only to a shift along the abscissa, and the size dependence of  $P_z(\theta)$  can be represented by a single curve. For a given structure type, a set of model scattering curves for different polydispersities is thus obtained. Applying this procedure, the first step consists in the choice of the appropriate model curve from the set of master curves. As for particle sizes of 100 nm and above, the curves differ significantly for the different basic structure types (spheres, coils, wormlike chains, rods) and, for a given structure type, with the polydispersity, the experimental curve can be assigned to a model curve. Having achieved a good fit, one obtains directly the size parameter and the value of  $M_w$  from the position of the experimental curve relative to the theoretical one. For wormlike chains, the characteristic size parameter is the persistence length  $L_p$ . The fit supplies  $L_w/L_p$  and  $\sigma_M$  from the choice of the model curve used for fitting and  $L_p$ ,  $M_w$ , and  $R_g$  from the position of the experimental curve on the theoretical one. Thus, one obtains the contour length  $L_w$  by multiplying  $L_w/L_p$  by  $L_p$ , and hence the mass per unit length  $M_L = M_w/L_w$ . In our model curves,  $\sigma_M$  is related to a logarithmic distribution of the contour length (see above). The fitting procedure is performed by means of a special PC program. For more details of the application to polysaccharides (pectin, xylinan), the reader is referred to refs (25–27). The wormlike chain interpretation has been applied in treating xylinan,<sup>26,27</sup> which is a close relative of xanthan by chemical structure and physicochemical behavior in aqueous solution.

The same xanthan sample has already been the subject of ultracentrifugation studies<sup>28</sup> at  $I = 0.3$  mol/L (phosphate buffer pH = 6.5 with added NaCl) which led to  $M_w = (5.9 \pm 1.1) \times 10^6$  g/mol and  $B = (3.4 \pm 0.3) \times 10^{-4}$  mL·mol·g<sup>-2</sup>. The behavior was found to be consistent with a highly extended and stiff conformation of the macromolecules. The intrinsic viscosity  $[\eta]$  was determined as  $(7534 \pm 2717)$  mL/g.

## Experimental Section

**Preparation of Solutions.** The xanthan sample (Keltrol, grade RD) was a commercial product (Kelco International, London, UK). The degree of substitution by pyruvate and acetate was given as 43.5 and 86.1%, respectively. The chemical composition was checked by gas–liquid chromatography after methanolysis,<sup>9</sup> confirming the purity.

The weighed amount of xanthan was dissolved overnight at room temperature under slight shaking. The desired amount of solid NaCl was then added<sup>2,11</sup> in small proportions. If indicated, the solutions were ultracentrifuged (Beckman L5 preparative centrifuge, ~90 min,  $45 \times 10^3$  rpm, 15–20 °C). The supernatant was separated from the precipitate by means of a syringe.

The polysaccharide concentrations were determined by the phenol–sulfuric acid method using glucose as a standard.

**Gel Permeation Chromatography.** The GPC equipment consisted of a Pharmacia column (2.6 cm diameter, 95 cm

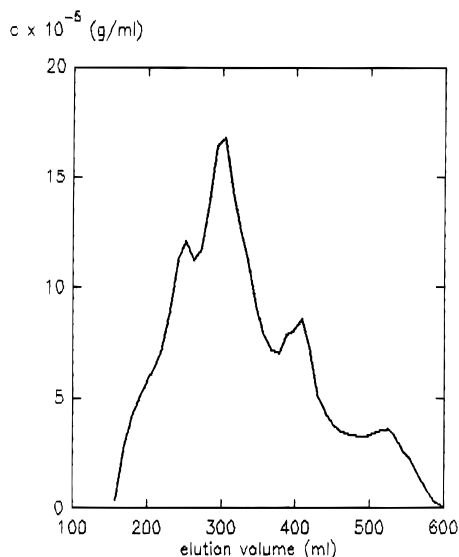


**Figure 1.** Elution profile of sonicated xanthan on Sepharose Cl-2B eluant: 0.10 M NaCl; void volume:  $\sim 150$  mL; total volume:  $\sim 500$  mL).

length) filled with about 500 mL of Sepharose Cl-2B, a peristaltic pump (P1, LKB, Sweden), a differential refractometer RID-6 (Shimadzu, Japan) calibrated with glucose, a ReCyChrom valve for the sample injection, and an UltraCac sample collector (all LKB Produkter, Sweden).

A sample volume of about 15 mL (2 mg/mL) was injected. Prior to injection, the solution was treated with ultrasonic waves (15 min under ice cooling, 100 W, Labsonic 1510 (Braun, Melsungen AG, FRG)). The flow rate was  $\sim 10$  mL/h. NaCl (0.1 M) was used as eluant and also as solvent (to prevent any salt peak near the total volume), and fractions of about 10 mL were collected. The fractions were filtered directly ( $0.45 \mu\text{m}$  pore size filter) into the dust-free measuring cell in the reverse order of their appearance for offline light scattering measurements.

**Static Light Scattering Measurements.** The measurements were performed in cylindrical cells using a SOFICA instrument (FICA, France), Model 42000, equipped with a 10 mW helium/neon laser (Uniphase, FRG) at an operating wavelength of 632.8 nm. The scattered light intensity was measured at 31 positions between 30 and  $150^\circ$ . In the case of GPC fractions, the scattering intensity was monitored only at 11 positions. The specific refractive index increment  $\delta n/\delta c$  was taken to be 0.15 mL/g.

All membrane filters used for clarification were made of cellulose acetate (Sartorius-Membranfilter-GmbH, FRG).

## Results and Discussion

In order to get a fractionable sample solution of reduced viscosity, xanthan was degraded by sonication and then fractionated by GPC. The elution profile on Sepharose Cl-2B is shown in Figure 1, indicating a distribution of the polymer between the void volume and the total volume. The light scattering intensities were measured and the resulting scattering curves were fitted with wormlike chain type "master curves" for the low but finite concentrations given by GPC. In doing so, we followed strictly the procedure described for xylinan in detail.<sup>26</sup> Because of the interfering effects of the polydispersity  $\sigma_M$  and the structural parameter  $L_w/L_p$  on the shape of the scattering curves, there is a certain ambiguity in the fitting procedure. Since a first attempt, choosing a moderate polydispersity of  $\sigma_M = 0.5$  as a fixed parameter, had led to an estimate of  $L_p \approx 150$  nm, we attempted a refined fit trying to keep  $L_p = 150$  nm constant and varying  $\sigma_M$  and  $L_w/L_p$  instead. We have accepted a tolerance of  $\pm 5\%$  for  $L_p$ , which reduces

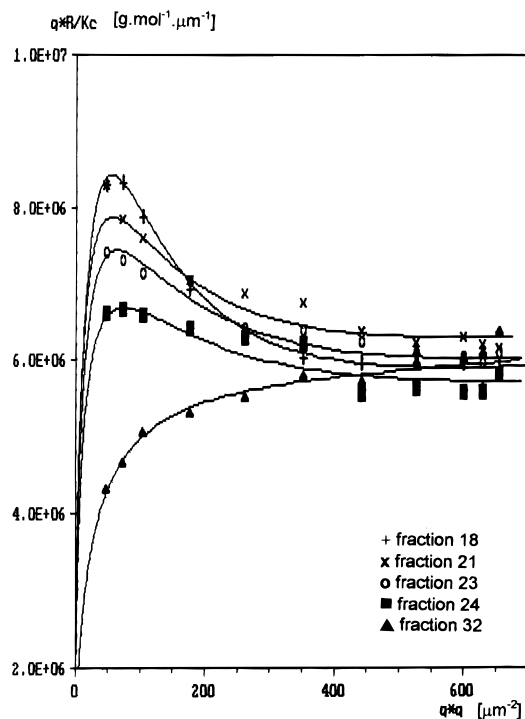


**Figure 2.** Holtzer plot for selected GPC fractions from Figure 1 (see also Table 1). The points denote experimental values, and the lines represent the model curves used for the fit.

the effort of the trial and error method (see also ref 3). The Holtzer plot<sup>29</sup> for some selected fractions in Figure 2 may illustrate the quality of fits achieved by the master curve procedure. The curves exhibit a characteristic shape with, eventually, a plateau region in the range of larger  $q$ -values. In our way of plotting, the height of the horizontal asymptote is  $1000\pi M_L$  (with  $q$  given as  $\mu\text{m}^{-1}$  and  $M_L$  as  $\text{g}\cdot\text{mol}^{-1}\cdot\text{nm}^{-1}$ ). This asymptotic region can thus be used for an estimate of the mass per unit length  $M_L$  (see, e.g., refs 2, 21, and 22). However, we have not made use of this fact but have computed  $M_L$  as described above. Results obtained by the master curve procedure are listed in Table 1. The molar masses  $M_w$  were measured in the range between  $2.6 \times 10^6$  and  $7 \times 10^5$  g/mol. Finally, taking the average over the fractions 17–39 and leaving out the questionable values in parentheses,  $L_p$  was calculated as 149 nm and  $M_L$  as  $1994 \text{g}\cdot\text{mol}^{-1}\cdot\text{nm}$ . The  $M_L$  value indicates double-stranded chains,<sup>2,5</sup> which is in accordance with the literature. Unlike  $L_p$ , neither  $M_w$  nor  $L_w$  has been found to be seriously affected by the choice of the model used for fitting due to the compensatory effects of changes in  $L_p$  and  $\sigma_M$ . Because of that,  $M_L$  can be estimated with a high level of confidence. But also  $L_p = 149$  nm appears to be reasonable in the context of data obtained by methodically quite different approaches.<sup>3–5</sup> It agrees well with results from another light scattering study.<sup>10</sup> The radius of gyration, however, does not vary in any sensible way with the fraction number in Table 1 and has been found to be the largest for the fractions which have the smallest molar masses. This effect is supposed to be caused by the strongly increasing polydispersities. Static light scattering is known to provide the  $z$ -average mean square radius of gyration, which stresses in particular the largest species within a distribution. If, for model calculations, pairs of  $M_w$  and  $L_p$  of the fractions with  $\sigma_M = 1.5$  were taken from Table 1 and  $R_{g,z}$  was calculated for wormlike chains with the hypothetical polydispersity of  $\sigma_M = 0.2$  instead,

**Table 1. Data for the GPC Run in Figure 1 and Results of the Interpretation of the Scattering Curves for the Individual Fractions by Means of Model Curves (Figure 2) with  $L_P = (150 \pm 7)$  nm as Parameter**

| no. of fraction | elution vol (mL) | $c \times 10^{-5}$ (g/mL) | $L_P$ (nm) | polydispersity |           | $M_w \times 10^{-6}$ (g/mol) | $R_g$ (nm) | $L_w$ (nm) | $M_L$ (g/mol·nm) |
|-----------------|------------------|---------------------------|------------|----------------|-----------|------------------------------|------------|------------|------------------|
|                 |                  |                           |            | $\sigma_M$     | $L_w/L_P$ |                              |            |            |                  |
| 16              | 157.0            | 0.4                       | —          | —              | —         | —                            | —          | —          | —                |
| 17              | 167.4            | 2.8                       | 143        | 0.20           | 9.5       | 2.60                         | 226        | 1359       | 1913             |
| 18              | 177.9            | 4.1                       | 145        | 0.20           | 7.5       | 2.06                         | 192        | 1088       | 1891             |
| 19              | 188.4            | 5.0                       | 145        | 0.30           | 7.0       | 1.89                         | 194        | 1015       | 1865             |
| 20              | 198.8            | 5.8                       | 152        | 0.50           | 7.0       | 2.15                         | 227        | 1064       | 2018             |
| 21              | 209.3            | 6.4                       | 155        | 0.65           | 6.5       | 2.04                         | 238        | 1008       | 2026             |
| 22              | 219.8            | 7.3                       | (168)      | 0.70           | 7.0       | 2.43                         | 281        | 1176       | 2066             |
| 23              | 230.2            | 9.0                       | 145        | 0.75           | 7.0       | 1.96                         | 253        | 1015       | 1934             |
| 24              | 240.7            | 11.4                      | 149        | 0.80           | 6.5       | 1.76                         | 259        | 969        | 1820             |
| 25              | 251.2            | 12.1                      | 149        | 0.80           | 6.0       | 1.49                         | 259        | 894        | 1667             |
| 26              | 261.6            | 11.3                      | 155        | 0.80           | 5.5       | 1.59                         | 256        | 853        | 1864             |
| 27              | 272.1            | 11.8                      | 149        | 0.80           | 3.25      | 1.22                         | 178        | 484        | 2526             |
| 28              | 282.6            | 14.0                      | 155        | 0.80           | 3.5       | 1.54                         | 194        | 543        | 2839             |
| 29              | 293.0            | 16.5                      | 151        | 0.80           | 3.5       | 1.21                         | 189        | 529        | 2282             |
| 30              | 303.5            | 16.8                      | 146        | 0.80           | 3.0       | 1.02                         | 165        | 438        | 2322             |
| 31              | 314.0            | 14.4                      | 147        | 1.00           | 3.25      | 0.87                         | 222        | 478        | 1829             |
| 32              | 324.4            | 12.7                      | 149        | 1.00           | 2.75      | 0.89                         | 203        | 410        | 2177             |
| 33              | 334.9            | 11.3                      | 146        | 1.00           | 3.0       | 0.76                         | 221        | 459        | 1647             |
| 34              | 345.4            | 9.2                       | 150        | 1.00           | 3.25      | 0.71                         | 227        | 488        | 1446             |
| 35              | 355.8            | 8.0                       | 151        | 1.20           | 2.75      | 0.73                         | 271        | 415        | 1746             |
| 36              | 366.3            | 7.2                       | 150        | 1.20           | 2.0       | 0.88                         | 223        | 300        | (2930)           |
| 37              | 376.7            | 7.0                       | 150        | 1.50           | 2.0       | 1.14                         | 360        | 300        | (3813)           |
| 38              | 387.2            | 7.9                       | 150        | 1.50           | 2.0       | 0.81                         | 360        | 300        | (2697)           |
| 39              | 397.7            | 8.0                       | 150        | 1.50           | 2.0       | 0.80                         | 360        | 300        | (2667)           |
|                 |                  | ↓                         | ∅149       |                |           |                              |            |            | ∅1994            |

**Table 2. Effects of Clarification at Various Ionic Strengths Expressed as Recovery Ratios in Percent and Determined by the Phenol–Sulfuric Acid Method (See Also Ref 30)<sup>a</sup>**

| pore size of filters ( $\mu\text{m}$ ) | 10 mM NaCl <sup>b</sup> |             | 0.10 M NaCl <sup>b</sup> |             | 0.10 M NaCl <sup>c</sup> | 0.30 M NaCl <sup>b</sup> |             | 0.30 M NaCl <sup>c</sup> |
|--|-------------------------|-------------|--------------------------|-------------|--------------------------|--------------------------|-------------|--------------------------|
|  | original                | supernatant | original                 | supernatant |                          | original                 | supernatant |                          |
| unfiltered                             | 100                     | 100         | 100                      | 70          | 100                      | 100                      | 75          | 46                       |
| 8.0                                    | 94                      | 99          | 86                       | 69          | 59                       | 84                       | n.d.        | n.d.                     |
| 5.0                                    | 94                      | 98          | 79                       | 67          | 57                       | 83                       | n.d.        | 43                       |
| 1.2                                    | n.d.                    | 99          | 76                       | 62          | 54                       | 80                       | n.d.        | 39                       |
| 0.8                                    | 93                      | 93          | 77                       | 59          | 47                       | 73                       | n.d.        | n.d.                     |
| 0.45                                   | 85                      | 87          | 64                       | 45          | 38                       | 58                       | 63          | 35                       |
| 0.2                                    |                         |             | 56                       |             |                          |                          |             |                          |

<sup>a</sup> Initial concentration:  $\sim 1$  mg/mL. <sup>b</sup> The sample was dissolved in distilled water and NaCl was added subsequently. <sup>c</sup> The sample was dissolved directly in the NaCl-containing solvent.

the resulting  $R_{g,z}$  values were found to be reduced from 360 nm in Table 1 to about a fifth. Values of  $\sim 80$  nm for the major proportion in fractions at the end of elution would appear to be reasonable compared with  $\sim 200$  nm for the fractions at the beginning of elution. This means the increasing polydispersities within a GPC run can explain well the apparent anomaly. In fact, our results are indicative of an increasingly poorer separation toward later stages of elution. The steadily broadening distributions might be caused by rather high molecular weight constituents which penetrate or pass through the soft Sepharose gel with delay and leave the column finally together with their relatively low molecular weight relatives. The high viscosity of the injected sample solution suggests the assumption of nonideal conditions with respect to optimum separation.

Another critical factor is the neglected concentration dependence of the scattering curves prior to the interpretation. This item has been discussed elsewhere<sup>26</sup> and shall be treated only in brief. It has been shown that—provided the second virial coefficient  $B$  is available—the scattering curve for a single concentration can be corrected subsequently to zero concentration according to  $Kc/R(q)_{c=0} = Kc/R(q) - 2Bc$ . Beyond the expected effect on the molar mass, this operation has an effect on the shape of the scattering curve so that, for a given polydispersity, the increase in the molar mass is accompanied by a corresponding increase in the contour length whereas the persistence length remains

practically unchanged. Consequently, the wormlike chain parameters such as  $L_P$  and  $M_L$  are unaffected. Unfortunately, we have not determined our own  $B$  values for xanthan in 0.1 M NaCl. That is why we have used  $B$  values ( $B = f(M_w)$ ) published by Sato et al.<sup>3</sup> in order to assess the effect of  $B$  on the molar masses in Table 1. These  $B$  values are all in the order of magnitude as  $10^{-4}$  mL·mol<sup>-1</sup>·g<sup>-2</sup>. Increases in  $M_w$  up to almost 25% have been obtained.

Having estimated a reasonable value for  $L_P$  on relatively low molecular weight samples, we are going to deal with the high molecular weight parent sample. For reasons given above, the effects of salinity on the solubility should be studied first. Results expressed as recovery ratios (in percent of the original matter) upon variable conditions of clarification are collected in Table 2 and Figure 3. The experiments were performed as “successive filtration series” starting with membrane filters of a pore size of 8.0  $\mu\text{m}$  and ending with 0.45 or 0.2  $\mu\text{m}$ . The carbohydrate concentration was measured in the solution that had passed through the filter and in the supernatant of centrifugation, respectively, by means of the phenol–sulfuric acid method. Despite the methodical problems associated with ultrafiltration (especially because of concentration polarization; see the review in ref 30), the trends gathered from the literature have been fully confirmed: at a unique initial concentration of  $\sim 1$  mg/mL, acceptable recovery ratios of  $\sim 85\%$  were found only in 10 mM NaCl, no matter whether or

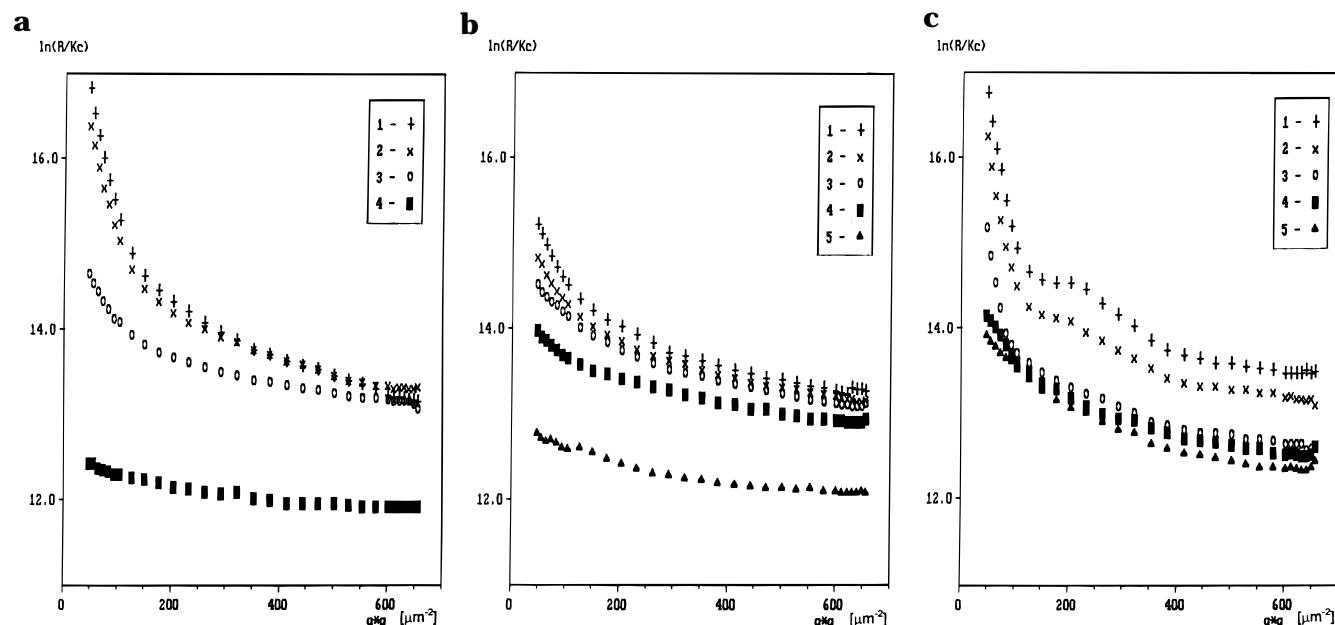


**Figure 3.** Guinier plot for the filtration tests: Effect of successive diminution of the pore size of membrane filters used for clarification (see also Table 2) [ $R/Kc$  given as g/mol]; initial concentration:  $\sim 1$  mg/mL. (a) Original solution (10 mM NaCl, 1.08 mg/mL): (1)  $8.0 \mu\text{m}$ , 1.01 mg/mL; (2)  $5.0 \mu\text{m}$ , 1.01 mg/mL; (3)  $0.8 \mu\text{m}$ , 1.00 mg/mL; (4)  $0.45 \mu\text{m}$ , 0.92 mg/mL. (b) Supernatant of centrifugation (10 mM NaCl, 1.08 mg/mL): (1)  $8.0 \mu\text{m}$ , 1.06 mg/mL; (2)  $5.0 \mu\text{m}$ , 1.05 mg/mL; (3)  $1.2 \mu\text{m}$ , 1.06 mg/mL; (4)  $0.8 \mu\text{m}$ , 0.99 mg/mL; (5)  $0.45 \mu\text{m}$ , 0.93 mg/mL. (5)  $0.45 \mu\text{m}$ , 0.93 mg/mL. (c) Original solution (0.10 M NaCl, 1.00 mg/mL): (1)  $8.0 \mu\text{m}$ , 0.86 mg/mL; (2)  $5.0 \mu\text{m}$ , 0.79 mg/mL; (3)  $1.2 \mu\text{m}$ , 0.76 mg/mL; (4)  $0.8 \mu\text{m}$ , 0.77 mg/mL; (5)  $0.45 \mu\text{m}$ , 0.64 mg/mL.

not the stock solution had been centrifuged. Centrifugation at higher ionic strengths removed considerable amounts of the original matter, which formed a colorless gel-like lense on the bottom of the tubes. Thus, in principle, all the higher ionic strengths studied drop out of the discussion. The differences between 0.1 and 0.3 M NaCl seem to be only slight. Also confirmed is the fact that the direct use of salt-containing solvents instead of initial dissolution in water followed by subsequently adding salt cannot be recommended because of the negative effect on the solubility (column 6, Table 2).

Parallel to the recovery ratios in Table 2, the light scattering intensities were measured as single-concentration studies. As representatives, the scattering curves in 10 mM NaCl are shown in Figure 3 when plotted according to Guinier.<sup>31</sup> This way of plotting has already been used in connection with filtration studies on several polysaccharides<sup>25,27</sup> and is based upon the relation

$$\ln \frac{R_\theta}{Kc} = \ln M_w + \ln P(\theta) \quad (5)$$

which can be derived from the basic equation (see, e.g., ref 32) if the concentration term is neglected. All notations have their usual meanings.<sup>32</sup>

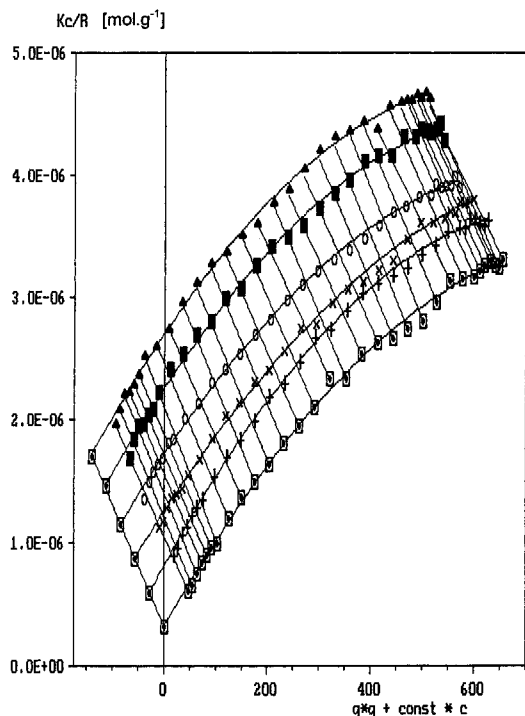
$P(\theta)$  describes the angular dependence of scattered light and depends on the shape, size, polydispersity, etc. of the scatterers. For  $\theta = 0$ ,  $P(\theta) = 1$  by definition so that the intercept of the scattering curve is equal to  $\ln M_w$  or, at finite concentration,  $\ln M_{w,app}$ . Therefore, a reduction in  $M_w$  corresponds to a downward shift of curves along the ordinate. A changing shape of curve is indicative of a change of size, shape, and of polydispersity of the system.

Panels a and b of Figure 3 reveal a steadily decreasing scattering level and, at the same time, a flattening of curves with diminishing pore size of the membrane filter used. This behavior indicates the stepwise removal of each of the largest species from the solution. After

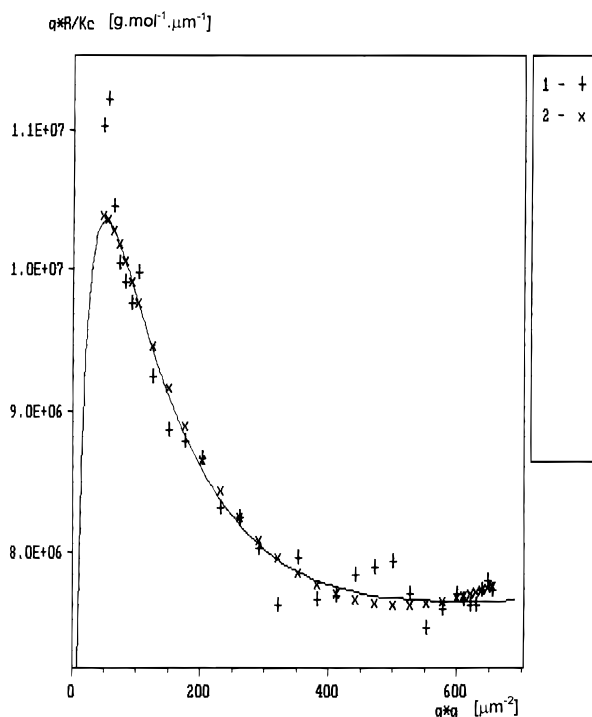
pretreatment by centrifugation, the same tendencies can be seen. Quite simply, the initial level and curvature have been reduced. The final scattering level after centrifugation/filtration through  $0.45 \mu\text{m}$  pore size filters is found to be a little higher and the curve appears a little steeper for a recovery ratio which is comparable with the uncentrifuged solution. However, there is a basic difference: While the centrifuged solution passed through the membranes without any problems, the untreated solution blocked the  $0.45 \mu\text{m}$  pore size filter rapidly. For only 20 mL of sample volume, the filter had to be renewed three times. This is not a good criterion for reproducible light scattering measurements. For that reason, the combination of centrifugation/filtration has been given preference.

Figure 3c gives an impression of the behavior of xanthan solutions of higher salinity upon membrane filtration. The  $8.0 \mu\text{m}$  pore size membrane was blocked rapidly (after the passage of only a few milliliters) but the subsequent filtration steps were performed without extreme (manual) pressure. The polymer retained formed a slimy layer on the filter surface. The shape of the curves 1 and 2 indicates the presence of large spherulike matter which disappears step-by-step in the order of decreasing pore size used for filtration. Nevertheless, after filtration through  $0.45 \mu\text{m}$  membranes, the scattering curve remains strongly curved and on a relatively high scattering level, suggesting rather complex solution behavior due to supermolecular structures (ref 12).

Based on the filtration tests described so far, a concentration series in 10 mM NaCl was studied for providing an estimate of  $M_w$ ,  $R_g$ ,  $B$ , and the scattering function at zero concentration. Therefore, the stock solution was centrifuged and filtered (twice) through a  $0.45 \mu\text{m}$  pore size membrane. The individual concentration steps were then filtered directly into the measuring cells in the order of increasing concentration (the blank solvent first). The resulting Zimm plot is given in Figure 4. A linear fit over the five measured



**Figure 4.** Zimm plot for xanthan in 10 mM NaCl ( $M_w = 3.12 \times 10^6$  g/mol,  $R_g = 264$  nm;  $B = 5.5 \times 10^{-4}$  mol·mL·g $^{-2}$ ).



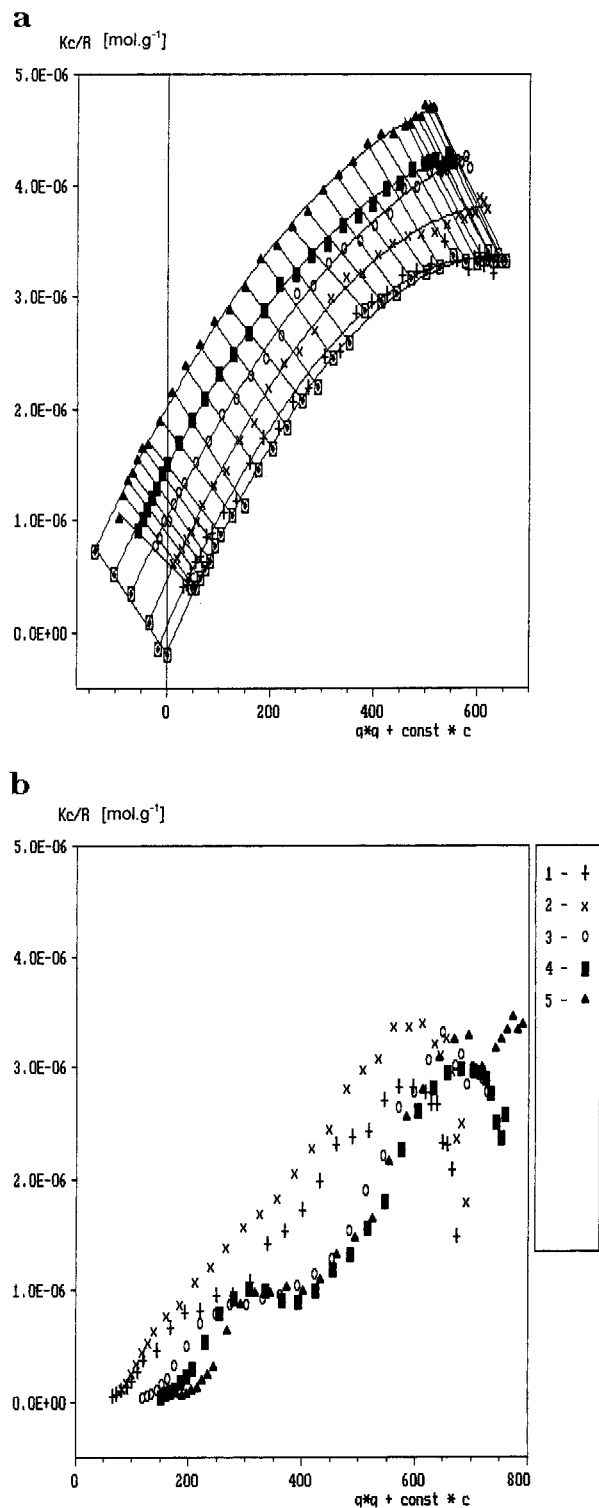
**Figure 5.** Holtzer plot: Model curve fit for the scattering curve at zero concentration from Figure 4: (+) directly from Zimm extrapolation; (x) "smoothed" curve from polynomial fit; (line) model curve used for the fit (for parameters, see text).

concentrations and a quadratic fit over all the 31 angles led to  $M_w = 3.12 \times 10^6$  g/mol,  $R_g = 264$  nm, and  $B = 5.5 \times 10^{-4}$  mL·mol·g $^{-2}$ . As already stated, the scattering curve is to be interpreted in terms of the wormlike chain model trying a fit with  $L_P = 150$  nm. The Holtzer plot in Figure 5 shows the extrapolated scattering curve for  $c \rightarrow 0$  from Figure 4. The symbol "+" marks the directly extrapolated points whereas the symbol "x" represents the corresponding "smoothed" scattering curve which results from the polynomial fit in Figure 4. The latter

could be fitted reasonably well with the model curve for the following set of parameters:  $L_P = 149$  nm,  $\sigma_M = 0.5$ ,  $L_w/L_P = 8.0$ ,  $M_w = 2.88 \times 10^6$  g/mol,  $R_g = 241$  nm,  $M_L = 2416$  g·mol $^{-1}$ ·nm $^{-1}$ . The deviations of the directly extrapolated points from the smoothed or model curves, especially for  $\theta \leq 35^\circ$  and  $\theta \geq 135^\circ$ , are of  $\sim 5\%$  and seem to reflect the somewhat reduced precision of measurements in this area. They are not supposed to indicate noticeable amounts of impurities. (The somewhat too high  $M_L$  value—compared with the calculated one for double-stranded chains as  $\sim 1950$  g·mol $^{-1}$ ·nm $^{-1}$ <sup>3</sup>—might be caused by the presence of side-by-side aggregates.) Thus, our data are obviously self-consistent although the GPC on the degraded xanthan was performed in 0.10 M NaCl. This would mean a small electrostatic contribution to the persistence length within our experimental accuracy of say 10 nm, which is in agreement with the findings of others<sup>33</sup> and is consistent with the theory for polyelectrolytes whose backbone has a high intrinsic inflexibility.<sup>34</sup>

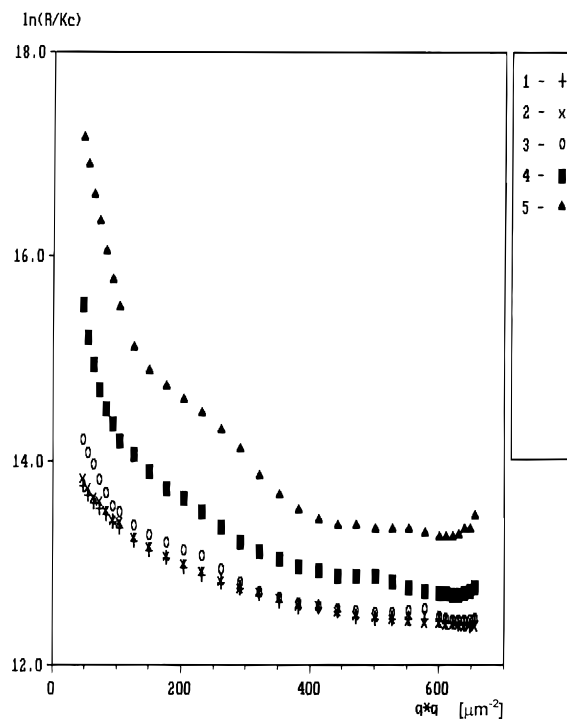
Parallel to the SLS measurements in 10 mM NaCl, the intrinsic viscosity  $[\eta]$  was determined as  $(2220 \pm 100)$  mL/g using the same set of clarified solutions in an Ubbelohde type viscometer at 20 °C. The filtration studies above (Table 2) and the comparison of our results from SLS in 10 mM NaCl and sedimentation analysis at  $I = 0.3$  mol/L<sup>28</sup> suggest the presence of largely associated material in solutions of higher salinity. This is supported by the big difference in the corresponding intrinsic viscosities of  $\sim 2220$  and  $\sim 7500$  mL/g, respectively. This means that high salinities must be avoided for the determination of molecular parameters. Nevertheless, it can be attractive to consider the behavior of solutions at higher ionic strength. For reasons of comparison, it appeared to be reasonable to check a concentration series at higher ionic strength also by SLS, expecting  $M_w$  and  $B$  data comparable to those from ultracentrifugation. The result of this can be seen in Figure 6. Figure 6a displays the Zimm plot for a freshly filtered set of solutions. It reveals distortions typical of bimodal systems:<sup>27,35</sup> the concentration dependence of  $dR_\theta$  decreases with decreasing angle of observation. The conventional interpretation of Zimm plots of that shape cannot be expected to give physically relevant average parameters and leads to a negative value of  $M_w$  in our special example. Sedimentation studies<sup>28</sup> had not given a hint for a complex situation as long as the polymer concentration was below 0.5 mg/mL. Frequently they allow us to assess the homogeneity of solutions.<sup>36</sup> Excellent agreement between the light scattering technique and sedimentation analysis was achieved elsewhere<sup>4</sup> when low molar mass samples with  $M_w$  below  $2.5 \times 10^4$  g/mol were studied in 0.1 M NaCl.

Figure 6b presents the corresponding Zimm plot for the same set of solutions after storage for 27 h at room temperature. Although the solution series had not visibly changed its appearance, the shape of the scattering curves indicates unambiguously the formation of large spherulike particles. They could be removed by a further filtration stage through a 0.45  $\mu$ m pore size filter so that the system reached a similar state to that before. Then the scattering behavior was monitored as a function of time. The results are given in Figure 7 (for the curve 4 from Figure 6 with  $c = 0.38$  mg/mL) corresponding to a period of 6 days. (The solution had become visibly turbid on the seventh day.) The Guinier plot illustrates the formation and growth of particles. This is indicated by the steadily increasing scattering level together with the increasing curvature from curve



**Figure 6.** Zimm plot for xanthan in 0.10 M NaCl: (a) fresh filtered; (b) after 27 h at room temperature.

1 toward curve 5. Comparable with the retrogradation of amylose,<sup>37</sup> this particle formation has shown itself to be an irreversible and continuing process. This will say that (i) particles which once had been formed could not redissolve upon heating (80 °C) and (ii) the process of particle formation went on and on even if particles had been removed in between. Particle formation was also observed on other xanthan preparations as well as in 10 mM NaCl solutions even for polysaccharide concentrations below 0.1 mg/mL. However, it could be prevented by storing the solutions at 80 °C. Although it had not been our intention to study temperature-



**Figure 7.** Particle formation with time over 6 days at room temperature in 0.10 M NaCl (Guinier plot,  $R/Kc$  given as g/mol).

driven conformation changes, some of our observations might be of interest in this context: (i) the clarified solutions in 10 mM NaCl did not change their scattering behavior after a heating step (1.5 h, 80 °C). (ii) The complex solutions in 0.10 M NaCl revealed also a complex behavior after heating, suggesting a two-component treatment of effects. The presence/formation of small amounts of particulate matter in polysaccharides is a widespread problem. A satisfying explanation cannot be given.

Some further experiments were carried out on partially hydrolyzed xanthans with truncated side chains. Such preparations had already gotten a heat treatment under mild acidic conditions.<sup>9</sup> Their solutions were stable over days or weeks at room temperature. When a sample such as no. 6 from ref 9 was studied in the same way as above (SLS coupled with GPC in 0.1 M NaCl; SLS standing alone in 10 mM and 0.1 M NaCl), a good fit was achieved with  $L_P = (125 \pm 10)$  nm and  $M_L \sim 1250 \text{ g}\cdot\text{mol}^{-1}\cdot\text{nm}^{-1}$ . Both the reduced persistence length and the mass per unit length for markedly degraded samples are in qualitatively good agreement with conclusions drawn from electron microscopy in combination with  $M_w$  data<sup>9</sup> from high-performance size exclusion chromatography with low-angle laser light scattering detection (HPSEC/LALLS).

Finally, it can thus be concluded that our findings on the conformation of xanthan in aqueous solution by static light scattering are in good accordance with data from the literature.

**Acknowledgment.** This work was supported by the Commission of the European Communities (Human Capital & Mobility Programme, Contract ERBCHB-GCT921040). G.B. thanks Dr. Bjørn T. Stokke, Department of Physics, University of Trondheim, for helpful discussions and lots of support in organizing the experimental work.

## References and Notes

- (1) Jansson, P. E.; Kenn, L.; Lindberg, B. *Carbohydr. Res.* **1975**, *45*, 275.
- (2) Paradossi, G.; Brant, D. A. *Macromolecules* **1982**, *15*, 874.
- (3) Sato, T.; Norisuye, T.; Fujita, H. *Macromolecules* **1984**, *17*, 1696.
- (4) Sato, T.; Norisuye, T.; Fujita, H. *Polym.* **1984**, *16*, 341.
- (5) Liu, W.; Sato, T.; Norisuye, T.; Fujita, H. *Carbohydr. Res.* **1987**, *160*, 267.
- (6) Liu, W.; Norisuye, T. *Biopolymers* **1988**, *27*, 1641.
- (7) Kawakami, K.; Okabe, Y.; Norisuye, T. *Carbohydr. Polym.* **1991**, *16*, 341.
- (8) Stokke, B. T.; Elgsaeter, A. In White, Ch. A., Ed.; *Advances in Carbohydrate Analysis*; JAI Press Ltd., London (England) and Greenwich, CT, 1991; Vol. 1.
- (9) Christensen, B. E.; Smidsrød, O.; Elgsaeter, A.; Stokke, B. T. *Macromolecules* **1993**, *26*, 6111.
- (10) Coviello, T.; Kajiwara, K.; Burchard, W.; Dentini, M.; Crescenzi, V. *Macromolecules* **1986**, *19*, 2826.
- (11) Gamini, A.; Mandel, M. *Biopolymers* **1994**, *34*, 783.
- (12) Hacche, L.; Washington, G. E.; Brant, D. A. *Macromolecules* **1987**, *20*, 2179.
- (13) Bezemer, L.; Ubbink, J. B.; Kooker, J. A.; Kuil, M. E.; Leyte, J. C. *Macromolecules* **1993**, *26*, 6436.
- (14) Kulicke, W. M.; Oertel, R.; Otto, M.; Kleinitz, W.; Littmann, W. *Erdöl Kohle, Erdgas, Petrochem., Hydrocarbon Technol.* **1990**, *43*, 471.
- (15) Kulicke, W. M.; van Eikeren, A. *Makromol. Chem., Macromol. Symp.* **1992**, *61*, 75.
- (16) Müller, G.; Lecourtier, J. *Carbohydr. Polym.* **1988**, *9*, 213.
- (17) Zimm, B. H. *J. Chem. Phys.* **1948**, *16*, 1099.
- (18) Koyama, R. *J. Phys. Soc. Jpn.* **1973**, *34*, 1029.
- (19) Norisuye, T. *Prog. Polym. Sci.* **1993**, *18*, 543.
- (20) Kratochvil, P. In Huglin, M. B., Ed.; *Light Scattering from Polymer Solutions*; Academic Press: London, New York, 1972.
- (21) Schmidt, M.; Paradossi, G.; Burchard, W. *Makromol. Chem., Rapid Commun.* **1985**, *6*, 767.
- (22) Denkinger, P.; Burchard, W. *J. Polym. Sci., Part B: Polym. Phys.* **1991**, *29*, 589.
- (23) Dautzenberg, H.; Rother, G. *J. Polym. Sci., Part B: Polym. Phys.* **1988**, *26*, 353.
- (24) Dautzenberg, H.; Rother, G. *Makromol. Chem., Makromol. Symp.* **1992**, *16*, 94.
- (25) Berth, G.; Dautzenberg, H.; Rother, G. *Carbohydr. Polym.* **1994**, *24*, 197.
- (26) Berth, G.; Dautzenberg, H.; Christensen, B. E.; Rother, G.; Smidsrød, O. *Biopolymers*, accepted.
- (27) Berth, G.; Dautzenberg, H.; Christensen, B. E.; Smidsrød, O. *Biopolymers*, accepted.
- (28) Dhami, R.; Harding, S. E.; Jones, T.; Hughes, T.; Mitchell, J. R.; Kar-mun, T. *Carbohydr. Polym.* **1995**, *27*, 93–99.
- (29) Holtzer, A. *J. Polym. Sci.* **1955**, *17*, 432.
- (30) Lee, S. *Trends Polym. Sci.* **1993**, *1*, 303–309.
- (31) Kerker, M. *The Scattering of Light and Other Electromagnetic Radiation*; Academic Press: New York, San Francisco, London, 1969.
- (32) Huglin, M. B., Ed. *The Scattering of Light from Polymer Solutions*; Academic Press: New York, London, 1972.
- (33) Zhang, L.; Liu, W.; Norisuye, T.; Fujita, H. *Biopolymers* **1987**, *26*, 333–341.
- (34) Dautzenberg, H.; Jaeger, W.; Koetz, J.; Philipp, B.; Seidel, Ch.; Stscherbina, D. *Polyelectrolytes—Formation, Characterisation and Application*; Hanser Publ.: München, Wien, New York, 1994.
- (35) Dautzenberg, H.; Rother, G. *J. Appl. Polym. Sci., Appl. Polym. Symp.* **1994**, *48*, 351.
- (36) Harding, S. E. *Prog. Colloid Polym. Sci.* **1994**, *94*, 54.
- (37) Pfannemüller, B.; Meyerhofer, H.; Schulz, R. C. *Biopolymers* **1971**, *10*, 243–261.

MA9515386